

QTabGAN: A Hybrid Quantum-Classical GAN for Tabular Data Synthesis

Subhangi Kumari¹, Rakesh Achutha², and Vignesh Sivaraman¹

¹ Department of Computer Science and Engineering, Indian Institute of Technology (BHU), Varanasi, India

² Department of Applied Mathematics and Theoretical Physics, University of Cambridge, Cambridge, United Kingdom

Synthesizing realistic tabular data is challenging due to heterogeneous feature types and high dimensionality. We introduce QTabGAN, a hybrid quantum-classical generative adversarial framework for tabular data synthesis. QTabGAN is especially designed for settings where real data are scarce or restricted by privacy constraints. The model exploits the expressive power of quantum circuits to learn complex data distributions, which are then mapped to tabular features using classical neural networks. We evaluate QTabGAN on multiple classification and regression datasets and benchmark it against leading state-of-the-art generative models. Experiments show that QTabGAN achieves up to 54.07% improvement across various classification datasets and evaluation metrics, thus establishing a scalable quantum approach to tabular data synthesis and highlighting its potential for quantum-assisted generative modelling.

1 Introduction

The rapid evolution of machine learning has transformed data-driven decision-making across various domains. Its impact is evident in various domains such as finance [1], healthcare [2], cybersecurity [3], transportation [4] [5], retail [6] [7], agriculture [8], manufacturing [9], and energy [10].

The growing need for privacy-preserving, scalable, and accessible data resources has made synthetic data generation an important focus in machine learning. Generative Adversarial Networks [11] are one of the widely used data generation techniques. In general, a GAN consists of a generator that generates synthetic data samples and a discriminator that evaluates the fidelity of these samples to the real data distribution. The GAN is trained in an adversarial setting until the discriminator is unable to distinguish between the generated data samples and the real data.

Traditional GANs perform well on continuous data such as images, but generating realistic tabular data remains difficult because real-world datasets often contain mixed discrete and continuous data [12] [13], complex and sparse distributions, high dimensionality, class imbalance [14], and intricate inter-feature dependencies. These factors collectively make synthetic tabular data generation significantly more challenging than continuous data synthesis. To address these challenges, several models have been proposed. CTGAN [12], introduces conditional generation and mode-specific normalization to more easily deal with mixed data types. TableGAN [15] is a GAN-based framework built to create synthetic tabular samples that retain the core statistical behaviour of the real data while reducing re-identification risks, thereby enabling safer data sharing. CTAB-GAN [16] and its improved variant, CTAB-GAN+ [17], incorporate dedicated encoders, downstream task-aware objectives, and differentially private training mechanisms to handle skewed feature distributions and class imbalance. CasTGAN [18] further extends the GAN framework through a cascaded architecture that synthesizes features sequentially, thereby improving dependency preservation and the overall validity of generated samples. In addition, domain-specific GANs have been proposed for applications such as healthcare and network security, demonstrating their effectiveness in generating realistic task-oriented tabular data [19] [20].

Despite these advancements, classical GANs often face challenges to effectively model the intricate distributions of complex tabular datasets, thereby limiting their utility in real-world tasks [21]. Quantum

Subhangi Kumari: subhangikumari.rs.cse24@itbhu.ac.in

Rakesh Achutha: ra741@cam.ac.uk

Vignesh Sivaraman: vignesh.cse@itbhu.ac.in

Generative Adversarial Networks utilizes the unique capabilities of quantum computing to enable more efficient representation and sampling of high-dimensional probability distributions [22] [23] [24]. This quantum advantage potentially overcomes the limitations of classical GANs by capturing complex correlations and generating high-fidelity synthetic tabular data[25] [26], thereby enhancing performance in various domains where classical approaches fall short due to their inability to fully capture the underlying data distribution. This makes Quantum GANs a compelling choice for overcoming the limitations of classical GANs, providing a more powerful framework for generating realistic synthetic data in real-world scenarios.

Quantum computing provides a promising direction for enhancing machine learning algorithms by exploiting principles such as superposition, entanglement, and quantum parallelism, that can offer computational advantages over classical approaches. Quantum GANs (QGANs) extend the GAN framework by using variational quantum circuits (VQCs) to model complex probability distributions [27]. Typically, a QGAN follows a hybrid approach where a quantum generator is paired with a classical discriminator that allows us to leverage the combined strengths of both computational paradigms.

Although early implementations of Quantum Generative Adversarial Networks (QGANs) have demonstrated strong potential, most existing literature has concentrated primarily on image-based generation, leaving tabular data generation largely unexplored. Recent studies primarily focus on image generation [28] [29] using datasets such as MNIST and Fashion-MNIST, while a few works explore time-series modelling for tasks like network-traffic anomaly detection[30].

In the context of tabular data, research in quantum generative modelling is still in its early stages, with TabularQGAN [31] representing one of the first exploratory attempts. While these preliminary efforts demonstrate potential, the existing literature still lacks a comprehensive framework that fully leverages the capabilities of quantum computing. This gap highlights the need for a Quantum GAN capable of capturing complex distributions and generating high-fidelity synthetic samples. To the best of our knowledge, we address this gap by presenting the first framework whose generative model fully utilizes quantum computational capabilities.

In this paper, we propose a novel Quantum Tabular Generative Adversarial Network (QTabGAN) that generates synthetic tabular data with high fidelity that is statistically representative and preserves label consistency. First, our model uses an n -qubit variational quantum circuit as the generator core to generate 2^n dimensional probability distributions. Next, we deploy a classical neural network to map these distributions to a tabular form. Ultimately, the discriminator serves as the adversary, distinguishing between real and synthetic data samples. To summarize, the main contributions of our work are as follows.

1. We propose a novel Quantum Tabular GAN framework (QTabGAN) that learns complex data distributions and inter-feature correlations, enabling the generation of high-fidelity, realistic synthetic tabular data.
2. Our model leverages the full expressiveness of quantum circuits to enrich the latent representation, enabling the generator to explore complex feature spaces that classical models struggle to capture.
3. We conduct comprehensive evaluations across diverse real-world tabular datasets using multiple performance metrics, demonstrating that QTabGAN generates high-fidelity synthetic data that remains indistinguishable from real data, highlighting both its robustness and broad applicability across domains.

Our paper is structured as follows: Section 2 presents the preliminaries of quantum computing and provides a high-level description of Generative Adversarial Networks (GANs). Section 3 outlines the architecture of the QTabGAN model. Section 4 details the Experimental Setup, including the data pre-processing strategy, QTabGAN training dynamics and QTabGAN Evaluation. Section 5 presents the experimental results, including the dataset description, evaluation metrics, and a comparison of the proposed framework against classical as well as quantum baselines. Section 6 discusses the key findings. Section 7 highlights the limitations and identifies opportunities for subsequent research.

2 PRELIMINARIES

Quantum computing utilizes the principles of quantum mechanics to process information in ways that are unattainable for classical computers. Quantum bits (qubits) can exist in a superposition of the classical states 0 and 1, allowing them to represent and process multiple states simultaneously. In addition,

entanglement creates correlations between qubits, enabling coordinated behaviour across the system. Together, superposition and entanglement enable quantum computers to surpass the computational capabilities of classical machines for certain tasks.

2.1 Qubits and Superposition

A qubit is the fundamental unit of quantum information, represented as:

$$|\psi\rangle = \alpha|0\rangle + \beta|1\rangle,$$

where α and β are complex probability amplitudes satisfying $|\alpha|^2 + |\beta|^2 = 1$. The ability of a qubit to exist in both states (i.e. $|0\rangle$ and $|1\rangle$) simultaneously enables quantum algorithms to explore multiple solutions concurrently.

2.2 Quantum Entanglement

Entanglement is a quantum phenomenon where the state of one qubit is intrinsically correlated with another, independent of their distance. A maximally entangled two-qubit Bell state is given by

$$|\Phi^+\rangle = \frac{1}{\sqrt{2}}(|00\rangle + |11\rangle).$$

Entanglement is an essential resource for quantum computing, enabling complex correlations that classical systems cannot efficiently replicate.

2.3 Quantum Gates and Circuits

Quantum gates serve as the fundamental building blocks of quantum circuits. They are unitary operators applied to one or more qubits to perform quantum computations, thereby evolving their states within a complex Hilbert space. Some of the most fundamental gates include:

- **Hadamard Gate (H):** This gate creates an equal superposition of the computational basis states. Its action on the basis state $|0\rangle$ and $|1\rangle$ is given by:

$$H|0\rangle = \frac{1}{\sqrt{2}}(|0\rangle + |1\rangle), \quad H|1\rangle = \frac{1}{\sqrt{2}}(|0\rangle - |1\rangle).$$

- **Rotation Gates (Rx, Ry, Rz):** These gates are single-qubit rotation gates that rotate a qubit's state around the x, y, or z-axis of the Bloch sphere by an angle θ .

$R_x(\theta)$: The R_x gate represents a rotation of a qubit state about the x -axis of the Bloch sphere by an angle θ . It is a single-qubit unitary operation that coherently mixes the computational basis states $|0\rangle$ and $|1\rangle$. Its matrix representation is:

$$R_x(\theta) = \exp\left(-i\frac{\theta}{2}\sigma_x\right) = \begin{bmatrix} \cos(\theta/2) & -i\sin(\theta/2) \\ -i\sin(\theta/2) & \cos(\theta/2) \end{bmatrix}$$

$R_y(\theta)$: The R_y gate performs a rotation of a qubit state about the y -axis of the Bloch sphere by an angle θ . This single-qubit unitary transformation introduces a coherent mixing of basis states through real-valued amplitudes. Its matrix representation is:

$$R_y(\theta) = \exp\left(-i\frac{\theta}{2}\sigma_y\right) = \begin{bmatrix} \cos(\theta/2) & -\sin(\theta/2) \\ \sin(\theta/2) & \cos(\theta/2) \end{bmatrix}$$

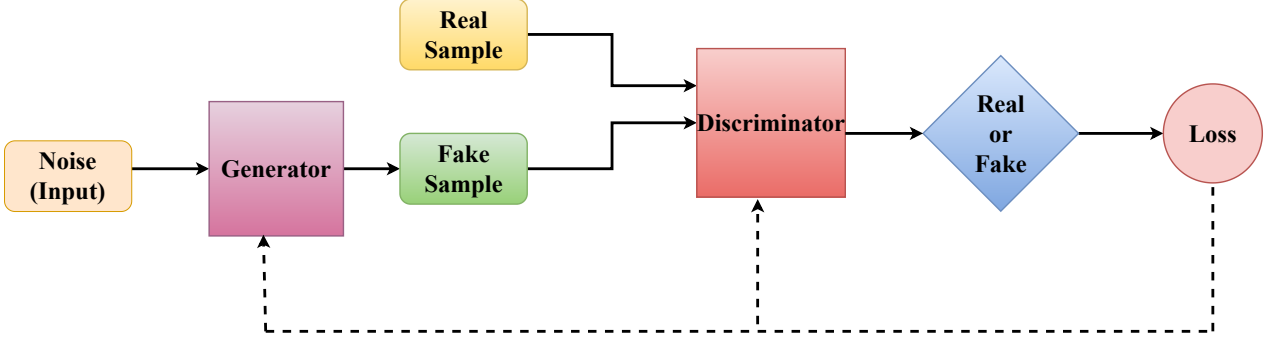


Figure 1: Basic Architecture of Generative Adversarial Networks (GANs)

$R_z(\theta)$: The R_z gate corresponds to a rotation about the z -axis by an angle θ . Unlike R_x and R_y gates, it applies relative phase shifts to the basis states while preserving their amplitudes. Its matrix representation is:

$$Rz(\theta) = \exp\left(-i\frac{\theta}{2}\sigma_Z\right) = \begin{bmatrix} e^{-i\theta/2} & 0 \\ 0 & e^{i\theta/2} \end{bmatrix}$$

- **Controlled-NOT (CNOT) Gate:** A two-qubit gate that flips the state of the output qubit if the control qubit is in state $|1\rangle$. It is essential for generating entanglement in quantum circuits:

$$\text{CNOT}(|a\rangle \otimes |b\rangle) = |a\rangle \otimes |a \oplus b\rangle, \quad a, b \in \{0, 1\}.$$

Quantum circuits are constructed by sequentially applying such gates to initialize, entangle, and transform quantum states in accordance with the computational task.

2.4 Variational Quantum Circuit

Variational Quantum Circuits (VQCs) are parameterized quantum circuits whose trainable gate parameters are optimized using classical optimization methods. They provide a flexible quantum ansatz capable of representing complex quantum states within a 2^n -dimensional Hilbert space. A general VQC acting on n qubits can be expressed as

$$|\psi(\theta)\rangle = U(\theta) |0\rangle^{\otimes n},$$

where $U(\theta)$ is a unitary operator parameterized by the set of angles θ . A common VQC design begins with an initialization layer often using Hadamard gates to generate superposition followed by layers of parameterized single-qubit rotations such as $R_Y(\theta)$ and $R_Z(\theta)$. Entanglement is introduced through controlled operations, most commonly using CNOT gates:

$$\text{CNOT}_{i,j} |q_i, q_j\rangle = |q_i, q_j \oplus q_i\rangle.$$

Following circuit execution, qubit measurements produce expectation values of chosen observables, which together define the objective function used during training. The parameters θ are iteratively updated through classical optimization strategies to refine the circuit's performance.

2.5 Generative Adversarial Networks (GANs)

Generative Adversarial Networks are a class of generative models that learn the underlying distribution of a dataset through adversarial training. Figure 1 represents the basic architecture of Generative Adversarial Networks (GANs). A GAN consists of two adversarial components: the generator that maps an input source such as random noise, conditioning information (e.g., class labels), or both together into synthetic data samples, and the discriminator that evaluates whether the given sample is real or synthetic. The neural networks are trained using an adversarial minimax objective where the generator aims to produce samples that the discriminator cannot distinguish, while the discriminator aims to improve its ability to distinguish between the real and synthetic data. This adversarial training enables the

generator to gradually synthesize high-fidelity samples that resemble the real-world data. The minimax objective function of a typical GAN is given as follows:

$$\min_G \max_D V(D, G) = \mathbb{E}_{x \sim p_{\text{data}}(x)} [\log D(x)] + \mathbb{E}_{z \sim p_z(z)} [\log(1 - D(G(z)))]$$

Here, x is a real sample and z is a synthetic sample. $D(a)$ is the probability that the discriminator tags a sample a to be real. The discriminator aims to maximize the first term, $\mathbb{E}_{x \sim p_{\text{data}}(x)} [\log D(x)]$, as the discriminator is supposed to identify the real samples with high probability. In the second term, $\mathbb{E}_{z \sim p_z(z)} [\log(1 - D(G(z)))]$, $G(z)$ is the sample generated by the generator and $D(G(z))$ is the probability that the discriminator tags the sample to be real. The discriminator aims to minimize this probability, while the generator attempts to maximize it.

3 Model Architecture

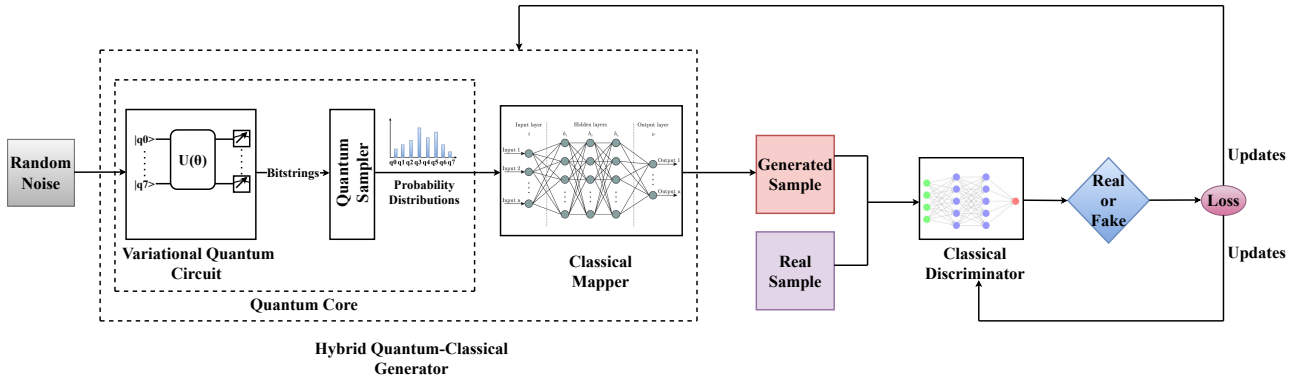


Figure 2: QTabGAN Model Architecture

Our proposed framework for QTabGAN is a hybrid quantum-classical framework. Figure 2 represents the model architecture of QTabGAN. The generator’s core is a Variational Quantum Circuit (VQC) that generates the probability distributions for synthetic data. VQCs are used to exploit quantum superposition and entanglement. This enables the generator to capture complex data distributions and correlations that classical generators struggle to capture. Next, the data distributions are mapped to the features of the tabular data using a classical neural network. Finally, the classical discriminator distinguishes between real and synthetic data.

3.1 Hybrid Quantum-Classical Generator Architecture

Our proposed Hybrid Quantum-Classical Generator is made up of three components, namely, the Variational Quantum Circuit (VQC), the Quantum Sampler, and the Classical Mapper (CLMapper). The VQC and the Quantum Sampler together form the generator’s core. The VQC learns the underlying probability distributions of the tabular data and the Quantum Sampler measures the VQC multiple times and gives probability vector. The CLMapper transforms these probability distributions into synthetic data.

3.1.1 Variational Quantum Circuit

The Variational Quantum Circuit (VQC) is configured with n qubits. Due to quantum superposition a VQC with n qubits yields a 2^n -dimensional Hilbert space where each dimension represent a feature of the tabular data. The VQC is constructed with a circuit depth of L layers. Each layer performs state initialization, parameterized rotations, and entanglement operations in the respective order. A single layer of the VQC for 8 qubits is shown in Figure 3.

First, to create a uniform superposition, we initialize each qubit by applying the Hadamard gate. This ensures a robust optimization starting point as all basis states are equally likely. The Hadamard gate is given as follows.

$$H^{\otimes n} |0\rangle^{\otimes n} = \frac{1}{\sqrt{2^n}} \sum_{x \in \{0,1\}^n} |x\rangle$$

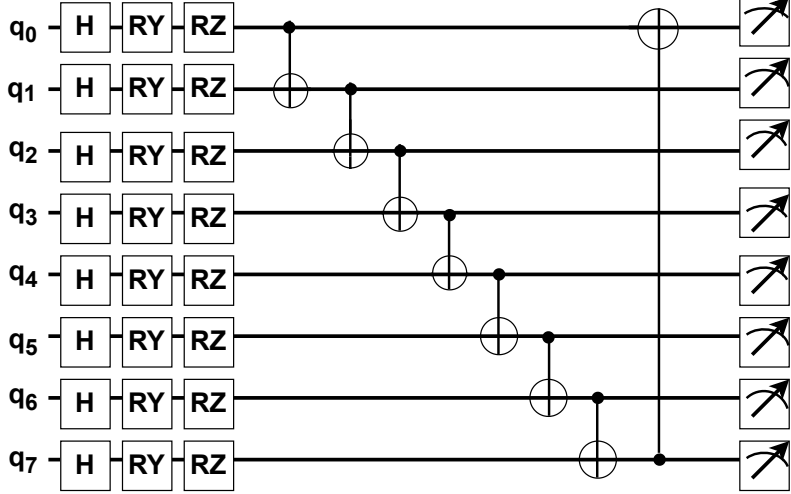


Figure 3: Variational Quantum Circuit Design

Next, for every qubit i in every layer l , we perform two parameterized rotations as follows. For each layer $l \in \{1, \dots, L\}$ and qubit $i \in \{1, \dots, n\}$, two parameterized rotations are applied as follows:

$$R_Y(\theta_{i,l}^Y) = \exp\left(-i\frac{\theta_{i,l}^Y}{2}\sigma_Y\right), \forall i \in \{1, \dots, n\}, \forall l \in \{1, \dots, L\}, (\theta_{i,l}^Y \mid \theta_{i,l}^Y \in_R [0, 2\pi])$$

$$R_Z(\theta_{i,l}^Z) = \exp\left(-i\frac{\theta_{i,l}^Z}{2}\sigma_Z\right) \forall i \in \{1, \dots, n\}, \forall l \in \{1, \dots, L\}, (\theta_{i,l}^Z \mid \theta_{i,l}^Z \in_R [0, 2\pi]).$$

Here, $\theta_{i,l}^Y$ and $\theta_{i,l}^Z$ are rotation parameters that are chosen randomly in the range $[0, 2\pi]$.

Finally, we form a circular entanglement of the qubits using CNOT gates. For every $i \in \{0, (n-2)\}$, we entangle the qubits i^{th} and $(i+1)^{\text{th}}$ and the $(n-1)^{\text{th}}$ qubit is circularly entangled with the 0^{th} qubit. We formally represent the circular entanglement as follows.

$$U_{\text{entangle}} = \prod_{i=0}^{n-1} \text{CNOT}(i, (i+1) \bmod n)$$

This circular entanglement enhances the VQC’s expressive power by (i) maximizing quantum correlations, (ii) enhancing quantum computational efficiency, (iii) and reducing circuit depth of the VQC [32]. All three factors together enable the VQC to efficiently capture complex data correlations and distributions. Another advantage of circular entanglement is that it achieves full entanglement across all the qubits with a minimal number of CNOT gates [33]. This makes it suitable for implementation on Noisy Intermediate-Scale Quantum (NISQ) devices (which are constrained by gate fidelity and coherence times). Once the minimax game of the GAN converges, the statistical properties of the data distribution are encoded in the parameters of the VQC.

3.1.2 Quantum Sampler

The quantum sampler is a measurement-based sampling module. This sampler generates samples from the parameterized probability distribution encoded in the quantum state of the VQC. To generate samples, the VQC’s quantum state is measured in the computational basis. The VQC is measured N ($N > 2^n$) times, and the empirical probability of each possible bitstring is evaluated. This gives us a probability vector of dimension 2^n . This probability vector is passed to the classical mapper, which maps the probabilities to the different features of the tabular data.

3.1.3 Classical Mapper

The Classical Mapper (CLMapper) is a classical feedforward neural network that transforms the probability vector p_θ into synthetic tabular samples. The generated samples have the same structure as the real dataset. Let c be the total number of class labels and d be the total number of attributes of the tabular dataset. Let $y \in \{0, 1\}^c$ denote the one-hot encoded class label of the synthetic data sample to be generated. We can then define the input to CLMapper, h_0 , as the concatenation of p_θ and y . Formally, h_0 is defined as follows.

$$h_0 = \begin{bmatrix} p_\theta \\ y \end{bmatrix} \in \mathbb{R}^{2^n + c},$$

The Classical Mapper is implemented as a multi-layer feedforward neural network with L layers whose input is h_0 . Let h_ℓ denote the output of the ℓ -th layer. For the hidden layers $\ell = 1, \dots, L - 1$, the transformation is defined as

$$h_\ell = \sigma(W_\ell h_{\ell-1} + b_\ell),$$

where W_ℓ and b_ℓ are the trainable weight matrix and bias vector of the ℓ -th layer, respectively, and $\sigma(\cdot)$ denotes the ReLU activation function. The vector h_ℓ represent intermediate feature representations learned by the Classical Mapper.

The final layer applies a linear transformation to produce the output

$$\hat{x} = W_L h_{L-1} + b_L, \quad \hat{x} \in \mathbb{R}^d.$$

Here, \hat{x} represents a generated synthetic tabular sample whose dimensionality matches that of the real dataset.

To summarize, the CLMapper takes in h_0 as input and generates the synthetic tabular sample \hat{x} as the output. The CLMapper is a relation from the Cartesian product of the probability distribution vectors and class labels to the attributes of the tabular dataset. We can formally define this relation as follows.

$$\mathcal{M}_\phi : \mathbb{R}^{2^n} \times \{0, 1\}^C \rightarrow \mathbb{R}^d.$$

3.1.4 Conditional Generation

Conditional generation in our framework enables explicit control over the class of generated tabular samples. This is achieved by concatenating the class label with the quantum-generated probability distribution as input to the Classical Mapper, enabling the generator to produce samples belonging to the desired class. As a result, the generator learns the conditional distribution $p(x | y)$, where x denotes the generated tabular feature vector and y denotes the corresponding class label, rather than the marginal distribution $p(x)$, ensuring that the generated samples are consistent with the provided class label. This conditioning helps address class imbalance in tabular datasets and reduces the risk of mode collapse, by encouraging the generator to produce more diverse samples. Mode collapse is a issue in generative models where the generator would output only limited varieties of data.

The resulting class-conditioned synthetic tabular samples are then forwarded to the discriminator as part of the adversarial training and evaluation pipeline.

3.2 Discriminator Architecture

The discriminator is a densely connected classical feedforward neural network designed to distinguish real tabular samples from synthetic samples generated by the hybrid quantum-classical generator during adversarial training. Figure 4 illustrates the discriminator architecture. The discriminator provides feedback to the generator, which guides the generator to produce synthetic samples that closely match the real data distribution.

The discriminator is a multi-layer feedforward neural network with L layers. Let h_ℓ denote the output of the ℓ -th layer. For the hidden layers $\ell = 1, \dots, L - 1$, the transformation is defined as:

$$h_\ell = \sigma(W_\ell h_{\ell-1} + b_\ell),$$

where W_ℓ and b_ℓ are the trainable weight matrix and bias vector of the ℓ -th layer respectively, and $\sigma(\cdot)$ denotes the ReLU activation function. The vectors h_ℓ represent intermediate feature representations

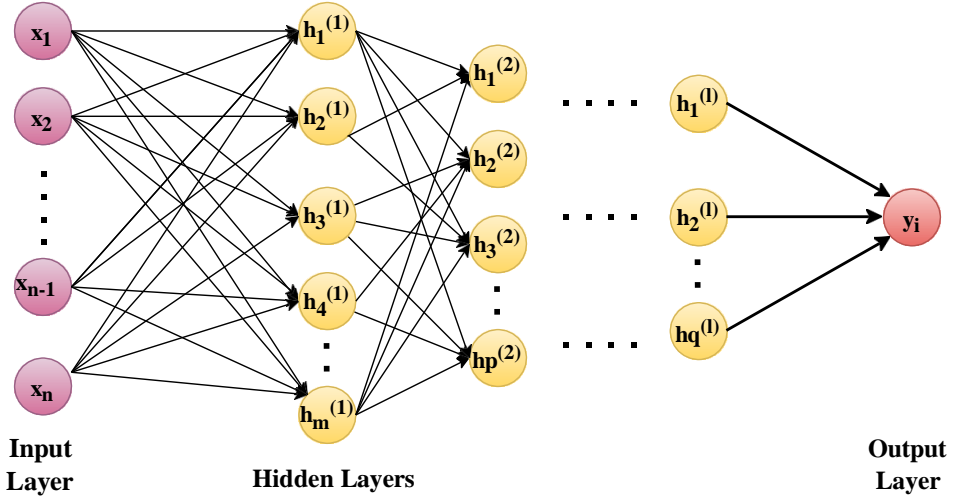


Figure 4: Discriminator Architecture

learned by the discriminator. The final layer applies a linear transformation to produce the discriminator output

$$D(x, y) = W_L h_{L-1} + b_L, \quad D(x, y) \in R.$$

Here, $D(x, y)$ denotes the scalar discriminator score assigned to the input sample, where x represents the tabular feature vector (real or generated) and y denotes the corresponding class label. This score is subsequently used to define the adversarial training objective through which the discriminator and the generator are jointly optimized during training.

4 Experimental Setup

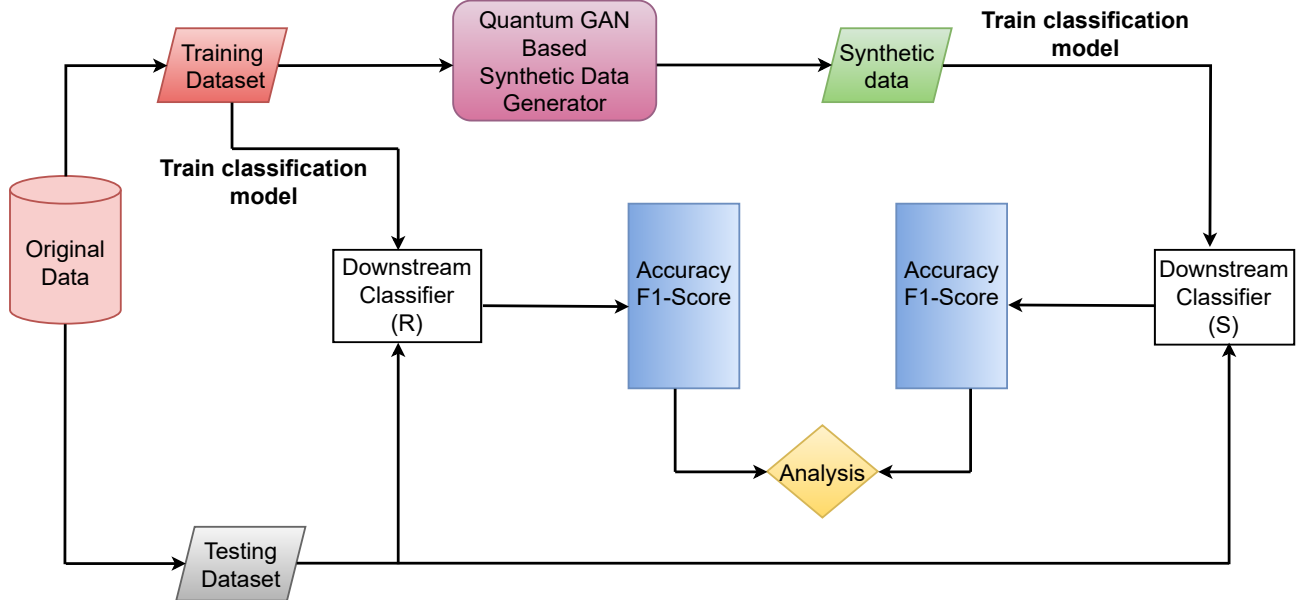


Figure 5: Evaluation flow for ML Utility of Classification datasets

4.1 Data Preprocessing

Data preprocessing is essential before training a model, as it enhances the quality and reliability of the dataset. This stage involves converting raw data into a clean and structured format, addressing issues such as missing values, noise, and inconsistencies. Proper preprocessing enables the model to learn more effectively, enhancing its ability to generalize and perform well on new data. The preprocessing of numerical features consists of the following steps.

1. We clip the feature values to the 1st and 99th percentiles. This minimizes the number of outliers and ensures numerical stability.
2. The second step is to use z-score normalization. We compute the mean μ and standard deviation σ of each feature and scale the feature value x to $x' = \frac{x - \mu}{\sigma + \epsilon}$, where ϵ is a small constant added to avoid division by zero.
3. Next, we perform min-max scaling that scales these features in the interval $[0, \pi]$. The scaled value x'' is evaluated as $x'' = \left[\frac{x' - \min}{\max - \min + \epsilon} \right] \cdot \pi$, where $\min(x')$ and $\max(x')$ denote the minimum and maximum values of the normalized feature across the training dataset.
4. Finally, we add Gaussian noise $\mathcal{N}(0, 10^{-5})$ to x'' to improve gradient stability and to reduce overfitting.

The preprocessing of categorial features primarily consists of converting the feature into a numerical format using one-hot encoding. In this process, each unique category within a categorical feature is represented as a binary vector. For a feature with multiple unique categories, the encoding creates a vector where the position corresponding to a specific category is marked with a 1, and all other positions are marked with 0s. This transformation is applied to each categorical feature, resulting in a set of binary vectors.

4.2 QTabGAN Training

The training process of QTabGAN follows an iterative adversarial learning procedure, which involves a hybrid quantum-classical generator and a classical discriminator. The overall training workflow is summarized as follows:

1. **Model Initialization:** The generator core, the classical mapper (embedded within the generator), and the classical discriminator are initialized. This includes initializing the parameters of the quantum circuit, the weights of the classical mapper, and the weights of the discriminator's neural network.
2. **Quantum Sample Generation:** The generator samples random noise and encodes it into the quantum circuit. The quantum circuit employs parameterized quantum gates, including rotation and entangling gates, to generate a quantum state (in the next step, the quantum sampler measures this quantum state).
3. **Probability Distribution Estimation:** The quantum sampler executes the quantum circuit for multiple number of shots and returns a probability vector over its measurement outcomes. This probability vector summarizes the stochastic measurement outcomes drawn from the learned quantum probability distribution of the hybrid quantum-classical generator.
4. **Classical Mapping and Conditional Generation:** The generated probability vector is concatenated with the corresponding one-hot-encoded class label and passed as input to the Classical Mapper. The Classical Mapper, implemented as a feedforward neural network, transforms this combined input into a synthetic tabular sample that matches the structure and dimensionality of the real dataset.
5. **Discriminator Evaluation:** The discriminator receives both real samples from the dataset and synthetic samples produced by the hybrid quantum-classical generator. It processes these samples through its layers and outputs a score indicating whether each sample is classified as real or synthetic.

6. **Loss Computation:** The discriminator loss is computed by comparing its predictions against the true labels (real samples labeled as 1 and synthetic samples labeled as 0) using an appropriate adversarial loss function. The generator loss is derived from the discriminator’s feedback, encouraging the generator to produce samples that are difficult for the discriminator to distinguish from real data.
7. **Gradient Computation:** Gradients of the loss functions are computed using the backpropagation algorithm. For the discriminator and the classical mapper, standard backpropagation is applied. For the hybrid quantum-classical generator, gradients with respect to the quantum circuit parameters are computed using hybrid techniques such as the parameter-shift rule, which enables gradient estimation for quantum operations [34].
8. **Parameter Optimization:** The parameters of both the generator and the discriminator are updated using the computed gradients. The discriminator’s parameters are updated to improve its ability to distinguish real and synthetic samples, while the generator’s quantum and classical parameters are updated to produce more realistic samples.
9. **Adversarial Update and Iteration:** The generator and discriminator are updated alternately in an adversarial manner, where the discriminator seeks to minimize its loss, and the generator seeks to maximize the discriminator’s loss. This process is repeated multiple times over several training iterations and epochs.
10. **Convergence:** Through repeated adversarial updates, the training process gradually converges toward a Nash equilibrium, where the generated synthetic samples become statistically similar to the real data, and the discriminator can no longer reliably distinguish between them.

4.3 QTabGAN Evaluation

The QTabGAN evaluation framework is shown in Figure 5. Our evaluation strategy follows established and widely adopted practices in synthetic tabular data generation, as used in prior works such as CT-GAN[12], CTAB-GAN+[17], and various other TabularGAN-based models. The framework is designed to assess both the utility and fidelity of the synthetic data produced by QTabGAN. The goal of this evaluation is to assess how well the synthetic data aligns with the statistical properties and predictive performance of the real data when applied in downstream machine learning tasks.

The evaluation workflow is summarized as follows:

1. Initially, the original dataset is first divided into two disjoint subsets: (i) the training subset and (ii) the testing subset.
2. The training dataset serves two purposes: (i) to train QTabGAN that generates synthetic data samples, (ii) to train the downstream classifier (R) for real data.
3. The QTabGAN is trained repeatedly on the training data until it converges, which helps the model to gradually learn the patterns and structure of the real data distribution.
4. Once trained, the model produces such synthetic dataset that replicates the properties of the real data distribution.
5. To evaluate the effectiveness of the synthetic data, two downstream classifiers are used: (i) trained on real data and (ii) trained on synthetic data generated by QTabGAN. Both classifiers are tested on the same unseen testing dataset to ensure a fair and unbiased comparison using metrics such as Accuracy and F1-score.
6. The machine learning utility of the synthetic data is measured by computing the absolute difference between the performance metrics obtained from both the downstream classifiers, given by

$$|\text{Metric}_{\text{real}} - \text{Metric}_{\text{synthetic}}|.$$

A smaller difference between the performance metrics of the two models indicates that the synthetic data closely mimics the real data and can be effectively used for downstream tasks.

7. Finally, Statistical similarity is evaluated by comparing the distributions and inter-feature relationships of real and synthetic data, where smaller differences indicate better preservation of real data characteristics.

5 Experimental Analysis

In this section, we first compare QTabGAN against state-of-the-art classical data generation methods, followed by a comparison with TabularQGAN, which, to our knowledge, is the only other published work on tabular data generation using quantum GANs.

5.1 Dataset Description

To evaluate our QTabGAN, we have used seven different datasets in total. The dataset descriptions are given below. The first two datasets are used for regression, while the remaining five are used for classification.

5.1.1 King Dataset

The King dataset contains the records of house sales in King County, Washington. It includes features such as house price, number of bedrooms and bathrooms, square footage of living and lot areas, floors, waterfront status, view, condition, and grade. We utilize ‘price’ as the target variable. The target variable represents the sale price of houses in King County. This dataset offers a rich source for analyzing housing prices in relation to structural, environmental, and geographical factors.

5.1.2 Insurance Dataset

The Insurance dataset used in this study contains records related to individual’s health and insurance information. It includes features such as age, gender, body mass index (BMI), number of children, smoking status, and residential region. We choose ‘charges’ as the target variable. The target variable represents an individual’s total medical expenses. This dataset can be used to examine how demographic and health-related factors influence insurance costs.

5.1.3 Adult Dataset

The Adult dataset used contains records of individual’s demographic and employment data. It includes features such as age, workclass, education, marital status, occupation, relationship, race, gender, capital gain, capital loss, hours worked per week, native country, and income level. We choose ‘income’ as the target variable. The target variable is binary, indicating whether an individual’s annual income is less than or equal to \$50,000 or greater than \$50,000. This dataset can be used to analyze patterns in income distribution across various socioeconomic factors.

5.1.4 Credit Dataset

The Credit dataset used in this study contains information about credit card transactions. It contains features such as time, amount, and twenty-eight other anonymized variables (V1-V28) derived from principal component analysis. This dataset aims to predict whether a given transaction is fraudulent. This dataset is generally used to learn patterns associated with fraudulent credit card behavior.

5.1.5 Intrusion Dataset

This dataset contains network traffic data for intrusion detection. It contains features such as duration, protocol type, service, flag, source and destination bytes, and various connection metrics, which aims at classifying network activities as normal or specific types of attacks. The dataset utilizes ‘attack_type’ as the target variable. The target variable is categorical, representing multiple classes corresponding to normal traffic and different types of network attacks. This dataset is ideal for analyzing patterns in network security threats due to its high dimensionality and diverse attack types.

5.1.6 Loan Dataset

The Loan dataset contains customer data from a financial institution. It includes features such as age, experience, income, ZIP code, family size, average credit card spending (CCAvg), education level, mortgage, securities account, CD account, online banking, and credit card usage. The dataset utilizes 'Personal Loan' as the target variable. The target variable is binary, indicating whether a customer's loan request is approved. This dataset can be used for learning patterns in credit risk analysis.

5.1.7 Covertype Dataset

The Covertype dataset used in this study contains records of forest cover type data from four wilderness areas in Colorado. It contains features such as elevation, slope, distances to hydrology, roadways, and fire points, hillshade indices, wilderness area, and soil type. The target is to predict the forest cover type, indicated by the name 'Cover_Type'. There are seven categories of forest cover type. This dataset is designed for classifying forest cover based on environmental variables, making it ideal for analyzing complex ecological patterns.

Dataset	Task	Train/Test Split	Target Variable	Dataset Size	Domain	Feature Count
King	Regression	80:20	Price	21,600	Real Estate	20
Insurance	Regression	80:20	Charges	1338	Healthcare and Insurance	7
Adult	Classification	80:20	Income	48,000	Socio-economic	14
Credit	Classification	75:25	Class	50,000	Finance	31
Intrusion	Classification	80:20	Attack_Type	50,000	Cyber Security	42
Loan	Classification	70:30	Personal Loan	5,000	Finance	13
Covertype	Classification	80:20	Cover_Type	50,000	Ecology	54

Table 1: Dataset Description.

5.2 Evaluation Metrics

We evaluate our proposed QTabGAN on two different evaluation paradigms. The first is the Machine Learning (ML) Utility for evaluating its predictive performance, and the second is Statistical Similarity for evaluating the distributional fidelity of the generated data. The different metrics used for these paradigms are described in the following subsections.

5.2.1 Machine Learning Utility

The Machine Learning (ML) Utility evaluates how well the synthetic data (generated by QTabGAN and other baseline models) supports downstream predictive tasks.

To test the performance of QTabGAN on classification datasets, we use the following metrics :

1. **Accuracy:** Accuracy is a classification metric that indicates how many predictions made by a model are correct compared to the total number of samples. Higher accuracy means the model predicts class labels more correctly.

The accuracy is computed as follows.

$$\text{Accuracy} = \frac{\text{TP} + \text{TN}}{\text{TP} + \text{TN} + \text{FP} + \text{FN}}$$

2. **F1-Score:** The F1-score is a classification metric that measures how well a model predicts class labels by considering both correct and incorrect predictions. It provides a single score that reflects overall classification performance, especially when the dataset contains imbalanced classes. A higher F1-score indicates better model performance. The F1-score is computed as follows.

$$\text{F1-Score} = \frac{2 \cdot \text{TP}}{2 \cdot \text{TP} + \text{FP} + \text{FN}}$$

To test the performance of QTabGAN on regression datasets, we use the following metrics :

1. **Explained Variance Score (EVS):** The Explained Variance Score (EVS) is a regression metric that measures how well a model explains the variation in the target variable. It demonstrates how well the model's predictions align with the actual data. A higher EVS value means the model captures more of the underlying variation in the target variable. The EVS is computed as follows.

$$\text{EVS} = 1 - \frac{\text{Var}(x - \hat{x})}{\text{Var}(x)}$$

where x is the actual value, \hat{x} is the predicted value, and Var denotes the variance.

2. **Coefficient of Determination (R^2):** The coefficient of determination (R^2) is a frequently used metric used to evaluate regression models. It measures how much of the variation in the target variable is explained by the model's predictions. Higher R^2 values indicate better model performance. The R^2 is computed as follows.

$$R^2 = 1 - \frac{\sum_{i=1}^n (y_i - \hat{y}_i)^2}{\sum_{i=1}^n (y_i - \bar{y})^2},$$

where y_i is the actual value, \hat{y}_i is the predicted value, \bar{y} is the mean of the actual values, and n is the number of observations.

After obtaining the above metric values for models trained on synthetic and real data, we compute the ML Utility Difference for the metrics as the absolute difference between the metric values obtained from synthetic and real data, $\text{Metric}_{\text{diff}} = |\text{Metric}_{\text{real}} - \text{Metric}_{\text{synthetic}}|$. The aim is to demonstrate the difference in ML utility when a model is trained on synthetic data versus real data. Smaller differences indicate that the synthetic data closely matches the predictive performance of the real data, making it a reliable substitute.

5.2.2 Statistical Similarity

The Statistical Similarity compares the distributions of synthetic and real data, assessing fidelity based on statistical properties. We use the following metrics to evaluate QTabGAN's performance.

1. **Jensen-Shannon Divergence (JSD):** The Jensen-Shannon Divergence (JSD) is a symmetric measure of similarity between two probability distributions, based on the Kullback-Leibler divergence. It is often used to compare distributions. Specifically, in the case of GANs, it is used to evaluate the quality of generated data. The JSD is computed as follows.

$$\text{JSD}(A||B) = \frac{1}{2} (D_{\text{KL}}(A||M) + D_{\text{KL}}(B||M))$$

where A and B represent the real and synthetic data distributions, and D_{KL} is the Kullback-Leibler divergence. The JSD, which is a symmetric and bounded metric, is calculated as Average JSD (Avg JSD). We compute the Jensen-Shannon Divergence (JSD) for each categorical feature and report the average value across all categorical columns as a single, interpretable score.

2. **Correlation Difference(Diff. Corr.):** The correlation difference metric measures how well the synthetic data preserves the pair-wise linear relationships between features present in the real dataset. It quantifies the average absolute deviation between the correlation matrices of the real and synthetic data. Smaller values indicate better structural similarity. The formula for Correlation Difference is given by:

$$\text{CorrDiff} = \frac{1}{K} \sum_{(i,j)} \left| \rho_{ij}^{\text{real}} - \rho_{ij}^{\text{syn}} \right|$$

where, K denotes the total number of unique feature pairs (i, j) , ρ_{ij}^{real} denotes the Pearson correlation coefficient between features i and j in the real dataset, ρ_{ij}^{syn} denotes the Pearson correlation coefficient between features i and j in the synthetic dataset, $|\rho_{ij}^{\text{real}} - \rho_{ij}^{\text{syn}}|$ represents the absolute difference in correlation for the feature pair (i, j) .

5.3 Result Analysis

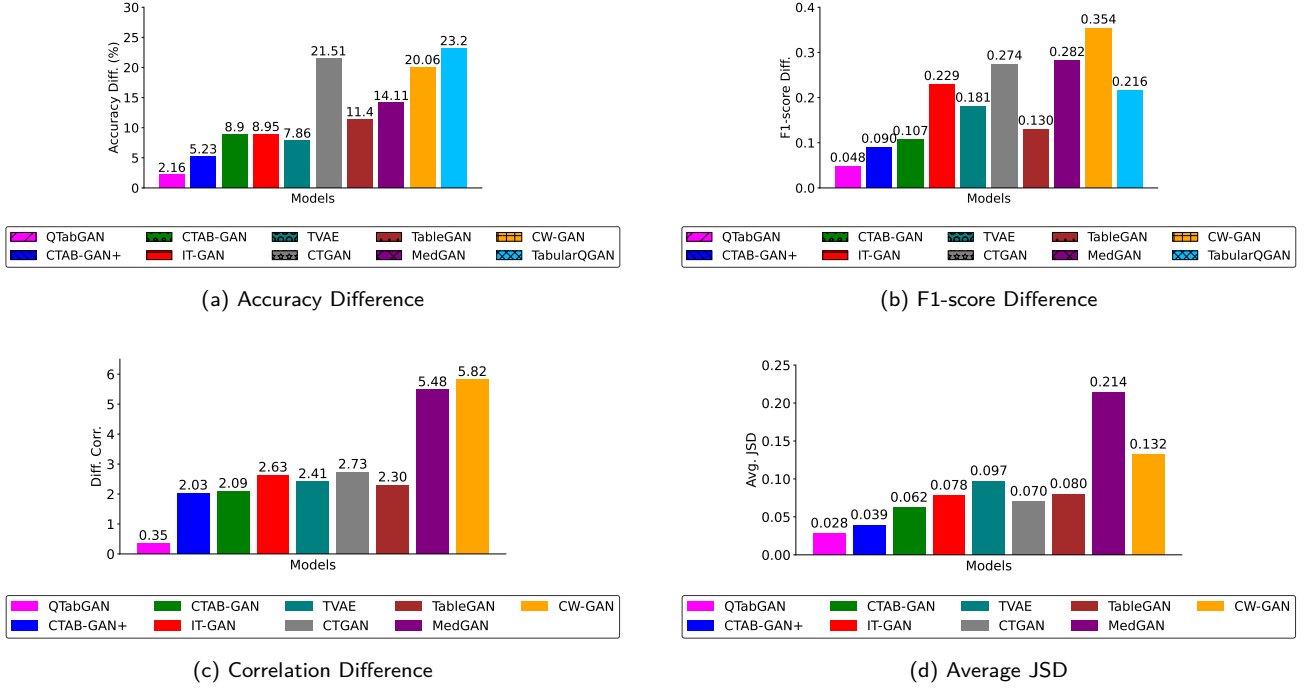


Figure 6: Difference in ML utility and statistical similarity between real and synthetic data, averaged across five classification datasets

Figure 6 and Figure 7 show the results for the classification and the regression datasets, respectively. For both classification and regression datasets, we compare QTabGAN against eight state-of-the-art generative adversarial network (GAN) models, namely, CTAB-GAN+, CTAB-GAN, IT-GAN, TVAE, CTGAN, TableGAN, MedGAN, and CW-GAN, to evaluate their relative performance across multiple metrics. Among these baselines, CTAB-GAN+ [17] is used as the main state-of-the-art baseline for comparison. We also compare QTabGAN against the TabularQGAN [31] model, which, to our knowledge, is the only other published work on tabular data generation using quantum GANs. For the comparison of ML utility metrics, QTabGAN is evaluated using the full set of features available in each dataset, whereas TabularQGAN is evaluated using a reduced subset of three to four features, as the TabularQGAN architecture does not scale to higher-dimensional feature spaces. In contrast, for the statistical similarity evaluation, both QTabGAN and TabularQGAN are assessed using the same subset of features to ensure a fair and consistent comparison, since these metrics are inherently feature-dependent whereas ML utility metrics does not depend upon number of features. For both classification and regression datasets, the results for each metric are obtained by averaging the corresponding metric values across all datasets. We first discuss the results on ML utility, followed by an analysis of statistical similarity.

5.3.1 ML Utility

The bar graph presented in Figure 6a illustrates the differences in accuracy (expressed in percentage). QTabGAN exhibits the lowest accuracy difference of 2.16%, indicating a relatively minor deviation in its performance. Compared to CTAB-GAN+ (5.23%) and CTAB-GAN (8.9%), QTabGAN demonstrates significant improvements, performing approximately 58.7% better than CTAB-GAN+ and 75.7% better than CTAB-GAN, reflecting a significantly lower accuracy difference. As compared to TabularQGAN, QTabGAN exhibits an accuracy difference of 2.16%, whereas TabularQGAN shows a substantially higher difference of 23.2%. QTabGAN demonstrates significant improvements, performing approximately 90.7%

better than TabularQGAN. This demonstrates that our model significantly outperforms both classical as well as existing quantum baseline in downstream performance.

The bar graph depicted in Figure 6b presents the differences in F1-scores (expressed as proportions). QTabGAN stands out with the smallest F1-score difference of 0.048, showing a highly consistent performance with minimal variation. In comparison to CTAB-GAN+ (0.090) and CTAB-GAN (0.107), QTabGAN shows remarkable enhancement, achieving approximately 46.7% superior performance over CTAB-GAN+ and 55.1% better performance over CTAB-GAN, indicating a significantly reduced F1-score difference. As compared to TabularQGAN, QTabGAN shows a smaller F1-score difference of 0.048, while TabularQGAN shows a F1-score difference of 0.216. This represents a 77.8% improvement in QTabGAN's performance as compared to the TabularQGAN model.

The bar graph presented in Figure 7a illustrates the absolute EVS Difference values. QTabGAN achieves the lowest EVS Difference of 0.02. In contrast, CTABGAN+ and CTABGAN exhibit higher EVS differences of 0.03 and 0.05, respectively. QTabGAN shows a remarkable improvement, achieving approximately 33% superior performance over CTABGAN+ and approximately 60% better performance over CTABGAN, showing that QTabGAN matches real-data prediction behaviour more closely. As compared to TabularQGAN, QTabGAN achieves a much lower EVS difference of 0.02, compared to 0.16 for TabularQGAN. This corresponds to an 87.5% improvement in QTabGAN's performance compared to TabularQGAN.

The bar graph presented in Figure 7b illustrates the absolute R^2 Difference values. QTabGAN achieves the smallest R^2 Difference of 0.02. Compared to CTABGAN+ and CTABGAN, which exhibit higher R^2 difference values of 0.04 and 0.06, respectively, QTabGAN achieves a remarkable improvement of approximately 50% over CTABGAN+ and approximately 66.7% over CTABGAN, indicating that QTabGAN better captures the variance of the real-data regression model. As compared to the TabularQGAN model, QTabGAN shows a smaller R^2 difference of 0.02, whereas TabularQGAN exhibits a substantially higher difference of 3.85. This shows an approximately 99.5% improvement in QTabGAN's performance compared to TabularQGAN.

A key limitation of the TabularQGAN model is that, for the same number of qubits, it can model only a small subset of features (typically three to four features), whereas QTabGAN is able to generate all features. This limitation directly affects the downstream performance of TabularQGAN, which can be seen in its consistently lower ML utility metrics across both classification and regression datasets. Furthermore, we can also observe that TabularQGAN does not even outperform classical models across the ML utility metrics.

From the results above, it can be seen that QTabGAN outperforms all other state-of-the-art methods across all ML utility metrics for both classification and regression datasets.

5.3.2 Statistical Similarity

The bar graph presented in Figure 6c presents the Correlation Difference scores for the classification datasets. QTabGAN achieves the lowest correlation difference of 0.35, indicating a stronger preservation of inter-feature relationships compared to the baseline models. This improved correlation preservation can be attributed to the use of entangling quantum circuits, which enhance the model's representational capacity for capturing feature dependencies. In comparison, CTAB-GAN+ and CTAB-GAN show higher deviations of 2.03 and 2.09, respectively. Compared to these two models, QTabGAN outperforms CTAB-GAN+ by approximately 82.76% and CTAB-GAN by approximately 83.25%.

The bar graph presented in Figure 6d presents the average Jensen–Shannon Divergence (Avg. JSD). QTabGAN achieves the lowest Avg. JSD of 0.028. In comparison, CTAB-GAN+ and CTAB-GAN show Avg. JSD scores of 0.039 and 0.062, respectively. Compared to these baselines, QTabGAN achieves significant improvements, reducing divergence by approximately 28.21% compared to CTAB-GAN+ and by 54.84% compared to CTAB-GAN, which demonstrates QTabGAN's superior ability to preserve the underlying data distribution.

The bar graph presented in Figure 7c presents the Correlation Difference scores for the regression datasets. QTabGAN achieves the lowest correlation difference of 0.22, indicating that it effectively preserves the relationships between features. In comparison, CTAB-GAN+ and CTAB-GAN show higher deviations of 0.65 and 1.23, respectively. Compared to these two models, QTabGAN outperforms CTAB-GAN+ by approximately 66.15% and CTAB-GAN by approximately 82.11%.

We also compare QTabGAN with the TabularQGAN model using statistical similarity metrics across both classification and regression datasets. To maintain a fair comparison in terms of statistical similarity, we evaluate similarity scores on the same features used by the TabularQGAN model for all the

datasets. Table 3 compares the statistical similarity between real and synthetic data generated by QTabGAN and TabularQGAN across both classification and regression datasets. Lower values indicate better alignment with the real data distributions.

For classification datasets, QTabGAN achieves a much lower average JSD of 0.05 compared to 0.20 for TabularQGAN. This corresponds to a 75% reduction in the difference between real and synthetic data distributions, indicating that QTabGAN more accurately captures the marginal feature distributions of the real data.

For classification datasets, QTabGAN achieves a lower correlation difference of 0.40 compared to 0.60 for TabularQGAN, resulting in an approximate 33.3% improvement in correlation preservation. This indicates that QTabGAN better preserves feature relationships, which helps the synthetic data to more accurately reflect the interactions present in the original dataset.

For regression datasets, QTabGAN achieves a lower correlation difference of 0.14 compared to 0.19 for TabularQGAN, resulting in an approximate 26.3% improvement in correlation preservation. This shows that QTabGAN more accurately preserves relationships among continuous features, which is important for regression tasks where feature dependencies strongly influence predictive performance.

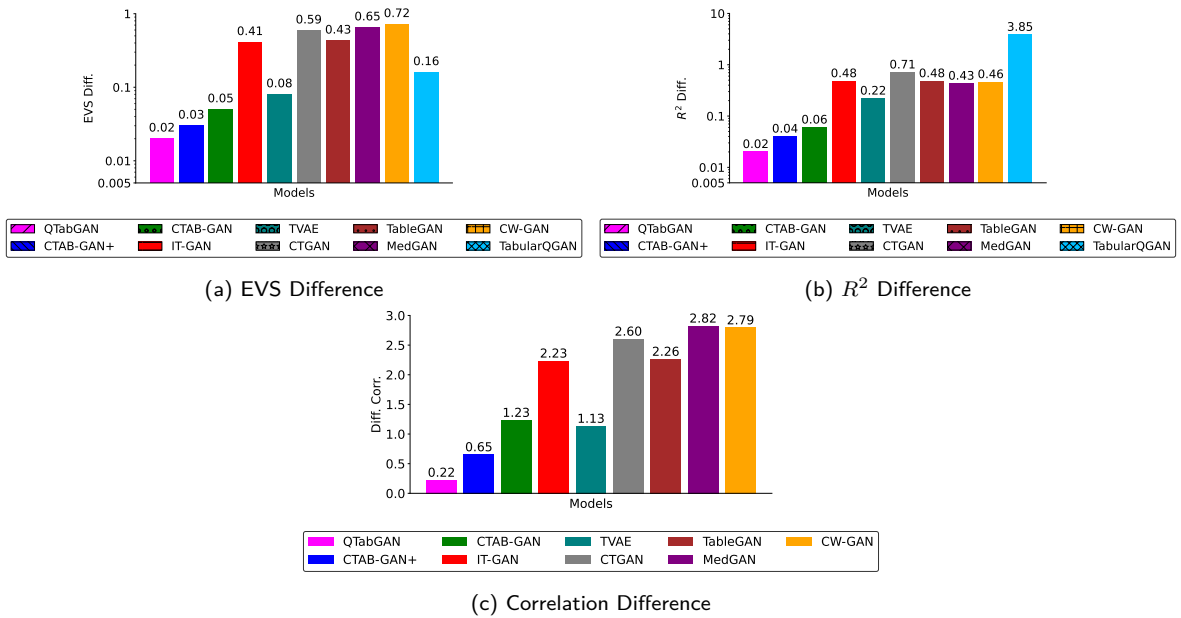


Figure 7: Difference in ML utility and statistical similarity between real and synthetic data, averaged across two regression datasets

From the above results for different metrics, it can be observed that QTabGAN outperforms all other state-of-the-art methods in all statistical similarity metrics for both classification and regression datasets.

QTabGAN achieves this strong performance on both classification and regression datasets due to its quantum-based design, which employs a variational quantum circuit to generate expressive probability representations. The hybrid architecture combines a variational quantum circuit with a classical mapping network, enabling the generation of full-feature tabular data in a scalable manner. These design choices allow QTabGAN to produce high-quality synthetic data that closely matches real-data behaviour, thereby reducing performance differences in downstream classification and regression tasks and demonstrating its effectiveness for tabular data generation.

Metric	Best			Worst		
	Real	Synthetic	Difference	Real	Synthetic	Difference
Accuracy	0.7760	0.7740	0.0020	0.9600	0.9380	0.0220
F1-score	0.7619	0.7539	0.0080	0.9570	0.9291	0.0279

Table 2: Best and Worst ML Utility Performance.

5.3.3 Best and Worst Case Analysis

Table 2 presents the accuracy and F1-score values obtained using real and synthetic data for the best-performing dataset (Adult) and one of the worst-performing datasets (Loan). For the Adult dataset, the differences in Accuracy and F1-score between models trained on real and synthetic data are the smallest among all classification datasets considered, indicating that QTabGAN’s synthetic samples closely match the underlying distribution of the real data.

In contrast, the Loan dataset exhibits relatively larger differences in both Accuracy and F1-score. This can be attributed to the smaller sample size and more complex feature relationships present in the Loan dataset. Despite its complexity, QTabGAN performs well on the Loan dataset. These results demonstrate that our model performs well across various types of datasets, ranging from simpler ones, such as the Adult dataset, to more complex ones, like the Loan dataset.

5.3.4 CDF-Based Distribution Analysis

Figure 8 presents smoothed cumulative distribution function (CDF) curves comparing real and synthetic samples for best and worst features across a classification and a regression dataset. CDFs provide an intuitive way to characterize data distributions, and smoothing helps reveal overall trends while reducing noise, enabling a clearer assessment of how well the synthetic data reproduces the statistical properties of the real data.

Sub-figure 8a and Sub-figure 8b show the best and worst CDF plots of the Adult dataset for age and capital-gain features, respectively. The CDF for the age feature shows a strong overlap between the real and synthetic data, indicating that QTabGAN effectively captures the overall distribution. For capital-gain, small differences are visible in some regions; however, the synthetic CDF closely follows the general cumulative trend of the real data. Such behaviour is expected for highly skewed and heavy-tailed features like capital-gain. Overall, QTabGAN preserves the main distributional characteristics across both smoothly varying and more challenging features, demonstrating stable and robust distributional learning.

Sub-figure 8c and Sub-figure 8d show the best and worst plots of the King dataset for sqft_living and yr_built features, respectively. The CDF for sqft_living15 closely matches the real and synthetic data, indicating that QTabGAN effectively captures the cumulative distribution. For yr_built, the CDF shows a smooth and monotonic trend, indicating that the proposed model is able to learn the overall distribution of the feature across its full range. The close alignment of the curves suggests that both lower and higher values are adequately represented, reflecting stable learning behaviour. These results show that the model preserves the global statistical characteristics in both cases and exhibits consistent performance across features in the King dataset.

Method	Classification Datasets		Regression Datasets
	Avg. JSD	Diff. Corr.	Diff. Corr.
QTabGAN	0.05	0.4	0.14
TabularQGAN	0.20	0.6	0.19

Table 3: Comparison of Statistical Similarity Differences for classification and regression datasets between original and synthetic data.

5.4 QTabGAN versus TabularQGAN: A Performance Perspective

In this section, we compare and contrast our work with TabularQGAN [31], which, to the best of our knowledge, is the only other work on tabular data generation in the quantum computing paradigm. First, we discuss the architectural advantages of QTabGAN that enable it to outperform TabularQGAN. Then, in the result analysis section, we also substantiate our arguments by comparing ML utility and Statistical similarity metrics. We note the following key architectural advantages of QTabGAN.

- TabularQGAN uses a full quantum generator, whereas QTabGAN uses a hybrid quantum-classical generator. In TabularQGAN, the features of the tabular data are encoded through dedicated quantum registers. As a result, the number of qubits required by the model grows linearly with the number of features to be generated. For example, to generate tabular data with 3 to 4 features, TabularQGAN requires 10 to 15 qubits. This increases the circuit size and computation cost. In

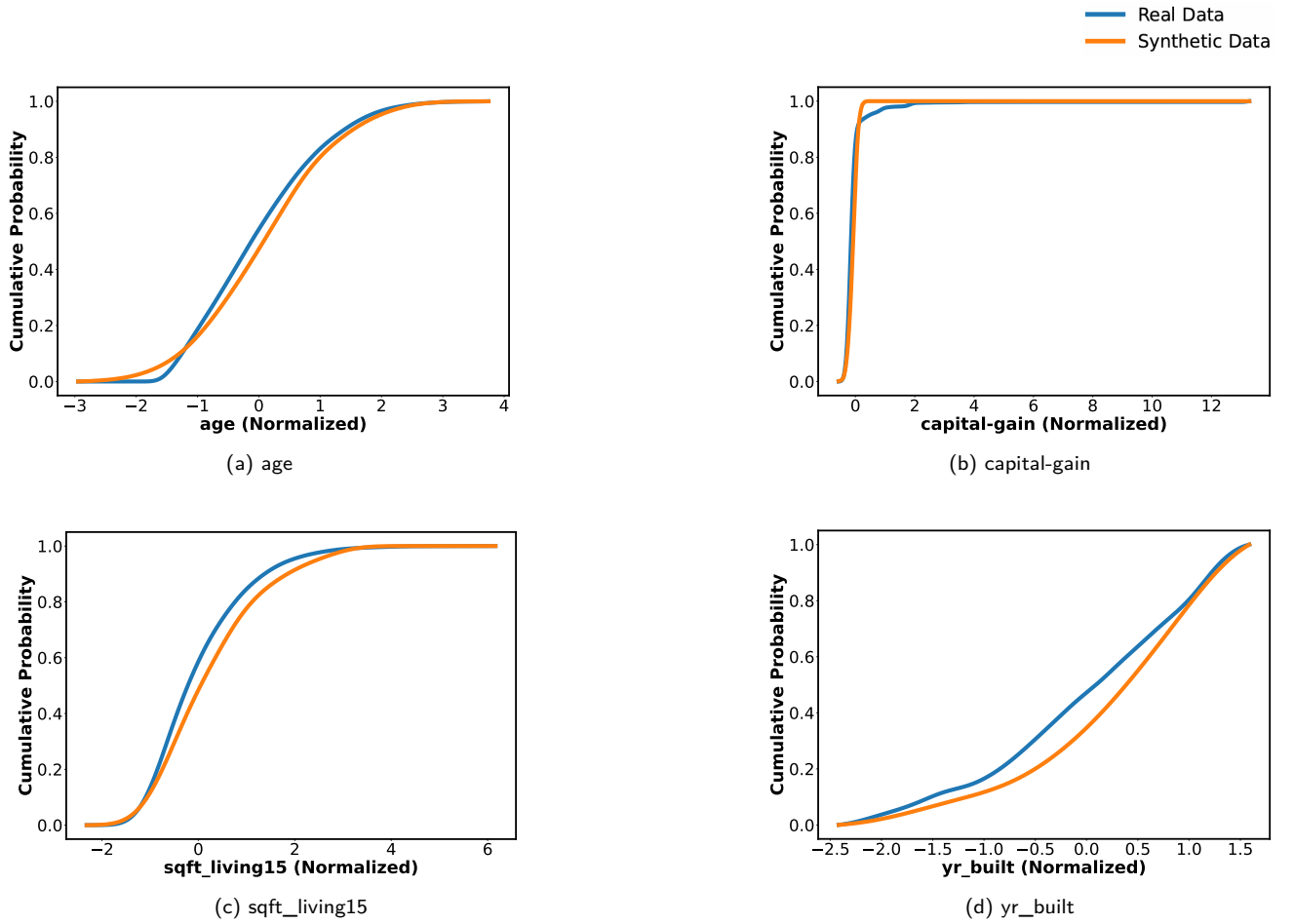


Figure 8: CDF visualizations for a subset of features from the Adult and King datasets. The figure includes four CDF plots corresponding to (a) age, (b) capital-gain, (c) sqft_living15, and (d) yr_builtin. The first two plots correspond to the Adult dataset, while the remaining two correspond to the King dataset.

contrast, QTabGAN uses a fixed number of qubits to generate a probability distribution over 2^n outcomes, which is then mapped to multiple tabular features using classical post-processing. This allows QTabGAN to represent and generate a larger number of features without increasing the number of qubits proportionally, making the model more scalable and efficient in terms of quantum resources.

- TabularQGAN represents numerical features using discretized qubit registers. This encoding approach divides continuous values into discrete quantum states, which restricts the resolution with which numerical ranges can be represented. QTabGAN avoids such binning by mapping features directly to the continuous interval $[0, \pi]$, allowing the quantum circuit and classical mapper to operate on smooth, full-resolution inputs.
- TabularQGAN has limited feature coverage due to the qubit overhead for feature-specific encoding. TabularQGAN experiments are limited to a small subset of features. As a result, only part of the available quantum state space can be explored. In contrast, QTabGAN generates a full 256-dimensional probability vector from its 8-qubit circuit, and its classical network learns relationships across all features in the dataset. This avoids feature-selection constraints and enables the model to capture broader patterns.
- QTabGAN’s hybrid structure makes it more suitable for present-day quantum hardware. By using fewer qubits and relying on classical neural networks for scalable learning, QTabGAN avoids the heavy qubit requirements and deeper circuits approach of TabularQGAN, reducing sensitivity to noise and making the model more practical for real-world synthetic tabular data generation.

5.4.1 NISQ Compatibility and Efficiency

QTabGAN is highly efficient for Noisy Intermediate-Scale Quantum (NISQ) devices. Specifically, QTabGAN is designed to operate with fewer qubits, fewer quantum gates, and a shallow circuit depth, factors that are critical for practical deployment on current quantum hardware. By employing a circular (ring) entanglement structure, the model leverages nearest-neighbour entangling operations, which have been shown to provide sufficient expressivity while limiting circuit depth and reducing noise accumulation in variational quantum circuits[35]. This architecture effectively reduces common NISQ bottlenecks such as decoherence and gate errors, thereby enhancing computational stability and fidelity. Consequently, QTabGAN not only achieves high-quality data generation performance but also maintains quantum resource efficiency, making it well-suited for implementation on near-term quantum devices. Due to limited access to quantum hardware and the high operational costs associated with current NISQ devices, all experiments were conducted on standard simulators, a widely adopted practice in contemporary quantum machine learning research.

6 Conclusion

This study demonstrates the effectiveness of our QTabGAN model for tabular data, which integrates a quantum circuit with classical neural networks to generate high-quality synthetic data for both classification and regression datasets. The proposed model not only leverages the expressive power of quantum circuits to capture intricate feature interactions in high-dimensional tabular datasets, but also utilizes classical deep learning components to ensure scalability and stability during training. The model showed strong predictive performance and favourable statistical similarity differences across diverse datasets. In our experiments, QTabGAN outperformed several classical generative baselines as well as the quantum baseline, demonstrating superior capability in producing synthetic data that closely matches real data. By embedding quantum circuits into the data generation process, the model effectively captures non-linear dependencies and complex probability distributions that are often difficult for classical models to represent. This property makes QTabGAN particularly valuable in scenarios where synthetic data must maintain a realistic structure. Overall, the results suggest that quantum-enhanced generative models can offer significant benefits in domains requiring secure and high-fidelity data synthesis, such as finance, healthcare, and IoT security. The ability of QGANs to balance utility along with generating realistic tabular data highlights their potential as a promising next-generation approach to synthetic data generation.

7 Limitations and Future Scope

Our model faces limitations due to the computationally expensive training of quantum circuits. As quantum hardware continues to grow in size and fidelity, performing training and sampling at scale on real quantum hardware would be valuable for understanding the impact of device noise on sample quality. Future work could explore more balanced hybrid configurations, as the incorporation of quantum components in the generator naturally increases its expressive capacity relative to the classical discriminator. Exploring architectures that combine these abilities may further improve training stability and generative performance.

References

- [1] Jian Huang, Junyi Chai, and Stella Cho. “Deep Learning in Finance and Banking: A Literature Review and Classification”. In: *Frontiers of Business Research in China* 14 (2020), pp. 12–13. DOI: <https://doi.org/10.1186/s11782-020-00082-6>.
- [2] Andre Esteva et al. “A Guide to Deep Learning in Healthcare”. In: *Nature medicine* 25 (2019), pp. 24–29. DOI: <https://doi.org/10.1038/s41591-018-0316-z>.
- [3] Abebe Abeshu Diro and Naveen Chilamkurti. “Distributed Attack Detection Scheme using Deep Learning Approach for Internet Of Things”. In: *Future Generation Computer Systems* 82 (2018), pp. 761–768. DOI: <https://doi.org/10.1016/j.future.2017.08.043>.
- [4] Abul Kalam Azad, Travis Atkison, and AFM Shah. “A Review on Machine Learning in Intelligent Transportation Systems Applications”. In: *The Open Transportation Journal* 18 (2024). DOI: <http://dx.doi.org/10.2174/0126671212330496240821114216>.
- [5] Mahbub Hassan et al. “Application of Machine Learning in Intelligent Transport Systems: A Comprehensive Review and Bibliometric Analysis”. In: *Discover Civil Engineering* 2 (2025), p. 98. DOI: <https://doi.org/10.1007/s44290-025-00256-2>.
- [6] Yuchen Wei et al. “Deep Learning for Retail Product Recognition: Challenges and Techniques”. In: *Computational intelligence and neuroscience* 2020 (2020), p. 8875910. DOI: <https://doi.org/10.1155/2020/8875910>.
- [7] Felix Weber and Reinhard Schütte. “A Domain-Oriented Analysis of the Impact of Machine Learning—The case of Retailing”. In: *Big Data and Cognitive Computing* 3 (2019), p. 11. DOI: <https://doi.org/10.3390/bdcc3010011>.
- [8] Dounya Knizia et al. “Harnessing Machine Learning for Transformation in Agricultural Sciences: A Review”. In: *Journal of Artificial Intelligence, Machine Learning, and Bioinformatics* (2025), pp. 16–28. DOI: <https://doi.org/10.5147/jaimlb.vi.256>.
- [9] Jinjiang Wang et al. “Deep Learning for Smart Manufacturing: Methods and Applications”. In: *Journal of manufacturing systems* 48 (2018), pp. 144–156. DOI: <https://doi.org/10.1016/j.jmsy.2018.01.003>.
- [10] Elena Mocanu et al. “Deep Learning for Estimating Building Energy Consumption”. In: *Sustainable Energy, Grids and Networks* 6 (2016), pp. 91–99. DOI: <https://doi.org/10.1016/j.segan.2016.02.005>.
- [11] Ian J Goodfellow et al. “Generative Adversarial Nets”. In: *Advances in neural information processing systems* 27 (2014). DOI: <https://doi.org/10.1145/3422622>.
- [12] Lei Xu et al. “Modeling Tabular Data using Conditional GAN”. In: *Advances in neural information processing systems* 32 (2019).
- [13] Akim Kotelnikov et al. “Tabddpm: Modelling tabular data with diffusion models”. In: *International conference on machine learning*. PMLR. 2023, pp. 17564–17579.
- [14] I Nyoman Mahayasa Adiputra and Paweena Wanchai. “CTGAN-ENN: a tabular GAN-based hybrid sampling method for imbalanced and overlapped data in customer churn prediction”. In: *Journal of Big Data* 11.1 (2024), p. 121. DOI: <https://doi.org/10.1186/s40537-024-00982-x>.
- [15] Noseong Park et al. “Data Synthesis Based on Generative Adversarial Networks”. In: *arXiv preprint arXiv:1806.03384* (2018). DOI: <https://doi.org/10.48550/arXiv.1806.03384>.
- [16] Zilong Zhao et al. “Ctab-gan: Effective table data synthesizing”. In: *Asian conference on machine learning*. PMLR. 2021, pp. 97–112.

[17] Zilong Zhao et al. “Ctab-gan+: Enhancing tabular data synthesis”. In: *Frontiers in big Data* 6 (2024), p. 1296508. DOI: <https://doi.org/10.3389/fdata.2023.1296508>.

[18] Abdallah Alshanti et al. “Castgan: Cascaded generative adversarial network for realistic tabular data synthesis”. In: *IEEE Access* 12 (2024), pp. 13213–13232.

[19] Malak Alqulaity and Po Yang. “Enhanced conditional GAN for high-quality synthetic tabular data generation in mobile-based cardiovascular healthcare”. In: *Sensors* 24.23 (2024), p. 7673. DOI: <https://doi.org/10.3390/s24237673>.

[20] Xinxing Zhao, Kar Wai Fok, and Vrizlynn LL Thing. “Enhancing network intrusion detection performance using generative adversarial networks”. In: *Computers & Security* 145 (2024), p. 104005. DOI: <https://doi.org/10.1016/j.cose.2024.104005>.

[21] Vadim Borisov et al. “Deep neural networks and tabular data: A survey”. In: *IEEE transactions on neural networks and learning systems* 35.6 (2022), pp. 7499–7519.

[22] Michael A Nielsen and Isaac L Chuang. *Quantum computation and quantum information*. Cambridge university press, 2010.

[23] Jacob Biamonte et al. “Quantum machine learning”. In: *Nature* 549.7671 (2017), pp. 195–202.

[24] Tuan A Ngo, Tuyen Nguyen, and Truong Cong Thang. “A survey of recent advances in quantum generative adversarial networks”. In: *Electronics* 12.4 (2023), p. 856. DOI: <https://doi.org/10.3390/electronics12040856>.

[25] Amira Abbas et al. “The power of quantum neural networks”. In: *Nature Computational Science* 1.6 (2021), pp. 403–409. DOI: <https://doi.org/10.5281/zenodo.4732830>.

[26] Maria Schuld and Francesco Petruccione. “Supervised learning with quantum computers”. In: *Quantum science and technology* 17 (2018). DOI: https://doi.org/10.1007/978-3-319-96424-9_8.

[27] Christa Zoufal, Aurélien Lucchi, and Stefan Woerner. “Quantum Generative Adversarial Networks for Learning and Loading Random Distributions”. In: *npj Quantum Information* 5 (2019), p. 103. DOI: <https://doi.org/10.1038/s41534-019-0223-2>.

[28] Su Yeon Chang et al. “Latent Style-Based Quantum GAN for high-quality Image Generation”. In: *arXiv preprint arXiv:2406.02668* (2024). DOI: <https://doi.org/10.48550/arXiv.2406.02668>.

[29] Daniel Silver et al. “Mosaiq: Quantum Generative Adversarial Networks for Image Generation on NISQ Computers”. In: *Proceedings of the IEEE/CVF international conference on computer vision*. 2023, pp. 7030–7039.

[30] Benjamin Kalfon et al. “Successive Data Injection in Conditional Quantum GAN applied to Time Series Anomaly Detection”. In: *IET Quantum Communication* 5 (2024), pp. 269–281. DOI: <https://doi.org/10.1049/qtc2.12088>.

[31] Pallavi Bhardwaj et al. “TabularQGAN: A Quantum Generative Model for Tabular Data”. In: *arXiv preprint arXiv:2505.22533* (2025). DOI: <https://doi.org/10.48550/arXiv.2505.22533>.

[32] Sukin Sim, Peter D Johnson, and Alán Aspuru-Guzik. “Expressibility and Entangling Capability of Parameterized Quantum Circuits for Hybrid Quantum-Classical Algorithms”. In: *Advanced Quantum Technologies* 2 (2019), p. 1900070. DOI: <https://doi.org/10.1002/qute.201900070>.

[33] Marc Hein et al. “Entanglement in graph states and its applications”. In: *arXiv preprint quant-ph/0602096* (2006). DOI: <https://doi.org/10.48550/arXiv.quant-ph/0602096>.

[34] David Wierichs et al. “General parameter-shift rules for quantum gradients”. In: *Quantum* 6 (2022), p. 677. DOI: <https://doi.org/10.22331/q-2022-03-30-677>.

[35] Marcello Benedetti et al. “Parameterized quantum circuits as machine learning models”. In: *Quantum science and technology* 4.4 (2019), p. 043001. DOI: <https://doi.org/10.1088/2058-9565/ab4eb5>.